JOURNAL OF PROPULSION AND POWER
Vol. 13, No. 3, May–June 1997

# Optical and Pressure Measurements in Shock Tunnel Testing of a Model Scramjet Combustor

T. J. McIntyre,* A. F. P. Houwing,† P. C. Palma,‡ P. A. B. Rabbath,§ and J. S. Fox§
*Australian National University, Canberra 0200, Australia*

**Experimental measurements are presented of the flow in a model supersonic–combustion ramjet. A rectangular duct with a central streamwise-injected planar hydrogen jet has been tested at various enthalpies in a free-piston-driven shock tunnel. Several optical diagnostic techniques were employed to characterize the flow for a moderate enthalpy condition where pressure measurements indicated that significant combustion was occurring. Shadowgraph and emission images provided qualitative information on the density variations and temperature distributions, respectively. The planar laser-induced fluorescence technique has been used to examine the regions of ignition. Combustion was found to be occurring only in a thin mixing layer present between the air and hydrogen streams. The positions of shock waves within the duct compared well with pressure measurements performed along the floor of the duct.**

## Introduction

THE successful development of the supersonic combustion ramjet (or scramjet) for use on future hypersonic vehicles is reliant on numerical and experimental studies that investigate the range of its operational envelope. Ground-based testing is a less expensive alternative to in-flight measurements and offers the capabilities of exploring operational characteristics as well as providing data for comparison with numerical codes. A major consideration in these studies is the mixing efficiency of the fuel and air during the relatively short residence time of the gases in the combustor. Improved mixing results in a shorter combustor section and improved engine efficiency.

Ground-based testing of flows relevant to these engines has been achieved in a number of forms. Basic research has focused on the study of compressible mixing layers (see, e.g., Hall et al.[1]), where growth rates as a function of velocity shear, density ratio, and compressibility were examined using schlieren techniques. More recently, the effect of heat release has been studied in coflowing streams of vitiated air and hydrogen using planar laser-induced fluorescence (PLIF) techniques to visualize the flow.[2] Investigations of partial and complete models of a scramjet using optical techniques have also been performed. An electrically heated air facility was used to study the sidewall injection of hydrogen into a low-enthalpy supersonic stream,[3] where PLIF was used to detect regions where OH was formed. Fluorescence imaging has been achieved in a shock tunnel facility at moderate enthalpies where PLIF was successfully implemented to probe NO and OH molecules present in the flow.[4]

Given that scramjets are likely to operate at velocities for which the total enthalpy ranges up to 18 MJ/kg, high-energy facilities such as free-piston-driven shock tunnels and expansion tubes are necessary to generate the full range of such conditions. Free-piston-driven shock tunnels, such as that used in this investigation, can provide a steady flow time of around 1 ms, simulating the conditions at the entrance to a scramjet duct. The equivalent flow densities and velocities are recreated, the only major deviation keeping it from being a complete simulation is the possible partial dissociation of oxygen molecules that occurs during the compression of the test gas by a strong shock. A number of studies in such facilities have been conducted to date with the emphasis mainly on surface and pitot pressure measurements. Casey and Stalker[5] measured pitot pressure profiles across the wake of a scramjet examining the spreading rate of the mixing layer present between the air and the fuel streams. Bélanger and Hornung[6] investigated the side injection of heated hydrogen into a hypersonic flow. They observed combustion and, by the use of resonant differential interferometry, were able to detect a reduction in the size of large-scale structures in the mixing layer. Bakos et al.[7] used pressure and heat-flux measurements to investigate the influence on the number and aspect ratio of injectors on the mixing and combustion processes. Most significantly, Paull et al.[8] used a force balance to measure the thrust and drag of a scramjet tested in the T4 shock tunnel. They demonstrated that a net thrust could be obtained for conditions where the enthalpy of the incoming flow lay in a suitable range.

A significant aid to such shock-tunnel testing is the application of two-dimensional optical diagnostic techniques. Such imaging can provide important information on shock locations, mixing layers, and combustion not otherwise obtainable from surface measurements. This paper presents results where surface pressure measurements have been combined with a range of optical techniques to study the flow in a scramjet duct tested in a free-piston driven shock tunnel. Experiments were conducted over a range of enthalpies with a centrally injected jet of cold hydrogen, including conditions similar to those used in the previously reported experiments that demonstrated a net thrust.[8] At conditions where pressure measurements indicated significant combustion, optical techniques were utilized to further investigate the flow. Shadowgraph imaging was used to provide the visualization of structures and shock waves. Emission measurements provided qualitative information on the temperature distribution in the flow. Most significantly, PLIF was used to visualize regions in the flow where the transient species OH was present, confirming that ignition was occurring and giving an indication as to the extent of mixing.

Received March 28, 1996; revision received Jan. 10, 1997; accepted for publication Jan. 14, 1997. 

*Research Fellow, Department of Physics, Faculty of Science; currently at Department of Physics, University of Queensland, Brisbane, Queensland 4072, Australia. Member AIAA.

†Senior Lecturer, Department of Physics, Faculty of Science. Member AIAA.

‡Postgraduate Student, Department of Physics, Faculty of Science. Student Member AIAA.

§Undergraduate Student, Department of Physics, Faculty of Science.

## Experimental Arrangement

### Scramjet Model

The model used for these experiments was a rectangular constant cross-sectional duct with a centrally injected hydrogen sheet representing the combustion region of the scramjet. The layout of the model is shown in Fig. 1. The duct has a 25 × 50 mm cross section and is about 400 mm in length. The injector is 5 mm thick, the upstream section of which forms the splitter plate that extended far enough into the flow so that shock waves generated at the tip passed outside the duct. Optical access was obtained via windows mounted in the side and top plates of the scramjet and test section. For shadowgraph measurements, float glass windows about 180 mm in length were flush mounted on each side of the scramjet. Because of the design of the model, images could only be recorded starting about 30-mm downstream from the injector. For PLIF and emission measurements, one of the side windows was replaced with a fused-silica window and a second fused-silica window was mounted in the top of the model. Pressure transducers were distributed along the floor of the duct beginning some 90-mm downstream from the injector as shown in Fig. 1. Kulite transducers were used, the signals of which were recorded on a LeCroy transient recorder at a rate of 250,000 samples per second. The precise positions of the transducers are given in Table 1.

Freestream conditions were generated in the free-piston-driven shock tunnel T3 (Ref. 9), using a nominal Mach 3 contoured nozzle with an area ratio of 12.1. Operation of this tunnel provides a range of conditions with a constant pressure test time of approximately 1–2 ms. The flow is terminated by the arrival of the driver gas that gradually mixes into the test gas. Injection of the hydrogen into the flow was achieved by the use of a Ludwieg tube and a fast-acting valve. The valve was triggered by detection of the recoil of the tunnel and set so that injection began several milliseconds before the arrival of the test gas and lasted well beyond the test time. The injector is designed with a throat several millimeters upstream of the injector exit that has dimensions 1.5 mm (height) × 49.2 mm (width). From this point the fuel was expanded in the vertical direction to a height of 3.2 mm giving an exit Mach number of about 2.3. Further changes can be expected as the pressure of the jet matches that of the airflow. This configuration thus provides an essentially two-dimensional flow with a sheet of hydrogen present between two coflowing sheets of test gas. The operating conditions for the tunnel and scramjet are given in Table 2. The initial shock-tube pressure, shock velocity, and nozzle reservoir pressure were measured from which the nozzle reservoir temperature was calculated using the equilibrium code ESTC.[10] The conditions at the exit of the contoured nozzle were then calculated using the one-dimensional nonequilibrium code, STUBE.[11] For comparison, the conditions at the inlet of the duct were measured by a pressure transducer mounted in the roof of the duct just upstream from the injector. The pressure and duration of the hydrogen flow were measured by a pressure transducer mounted just prior to the injector. Experiments were principally conducted with an equivalence ratio of about 1, as given in Table 2. (The equivalence ratio is the amount of fuel used divided by the amount required for stoichiometric burning.) However, a series of experiments was also conducted for a fuel lean condition with an equivalence ratio of 0.5.

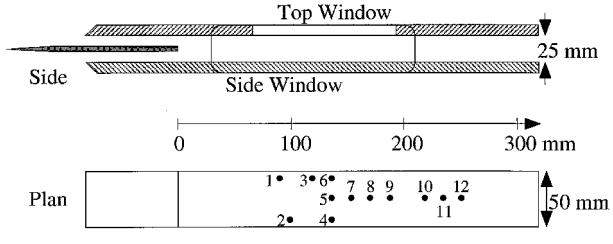


**Fig. 1 Schematic of the scramjet model showing dimensions, transducer positioning, and window locations.**

**Table 1 Pressure transducer locations**

| Pressure transducer | Distance from injector, mm | Normalized distance, to injector height |
|---|---|---|
| 1 | 90 | 28 |
| 2 | 100 | 31 |
| 3 | 120 | 38 |
| 4, 5, 6 | 137 | 43 |
| 7 | 154 | 48 |
| 8 | 171 | 53 |
| 9 | 188 | 59 |
| 10 | 218 | 68 |
| 11 | 235 | 73 |
| 12 | 252 | 79 |

**Table 2 Operating conditions**

| Enthalpy, MJ/kg | 4 | 8 | 12 |
|---|---|---|---|
| Nozzle reservoir | | | |
| Pressure, MPa | 15 | 15 | 15 |
| Temperature, K | 3200 | 5020 | 6580 |
| Freestream | | | |
| Pressure, kPa | 110 | 143 | 149 |
| Temperature, K | 1100 | 2490 | 3360 |
| Density, kg/m$^3$ | 0.36 | 0.20 | 0.15 |
| Velocity, m/s | 2390 | 3180 | 3730 |
| Mach number | 3.7 | 3.4 | 3.4 |
| Dissociation fraction O | 0.002 | 0.071 | 0.30 |
| Injector[a] | | | |
| Equivalence ratio | 0.92 | 0.96 | 1.0 |
| Fill pressure, kPa | 1300 | 1100 | 1100 |
| Fill temperature, K | 300 | 300 | 300 |
| Exit temperature, K | 150 | 215 | 170 |
| Exit density, kg/m$^3$ | 0.18 | 0.20 | 0.21 |
| Velocity, m/s | 2100 | 2200 | 1900 |

[a]Exit conditions calculated assuming a steady expansion to the freestream pressure.

### Shadowgraph System

A schlieren/shadowgraph system was employed to provide qualitative flow visualization to identify regions to be more closely examined by the other techniques. It has the advantage of being relatively easy to implement and provides a wide field of view. The system was a standard double-pass arrangement using a flashlamp-pumped dye–laser as a light source with images recorded on Ilford HP5 film. To operate as a schlieren system, a knife edge was inserted at the focus of the main mirror. However, after initial testing, it became obvious that the system was too sensitive, yielding images that were difficult to interpret. The knife-edge was replaced by a graded neutral density filter resulting in the observation of predominantly shadowgraph effects.

Triggering was achieved using the nozzle reservoir pressure transducer and employing a variable delay unit to observe the flow at different stages of the test time. The pulse length of the laser was some 500 ns, which was sufficiently short to produce an instantaneous image of the flow.

### Emission System

The principal apparatus for emission measurements was an in-house assembled intensified charge-coupled device (ICCD) camera designed for PLIF measurements. This unit consisted of a dual microchannel plate intensifier coupled by a fiber-optic to an asynchronous charge-coupled device (CCD) camera and is sensitive over the wavelength range of approximately 200–800 nm. Focussing was achieved with a Nikor uv lens (105 mm, $f$/4.5). The system is gateable down to about 150 ns, although gating times of about 250 ns were used for these

experiments. The geometry and resolution of the camera restricted the size of the images to the order of 50 × 25 mm. The flow was imaged onto the camera through a number of different filters in an attempt to identify the spectral region where emission signals were generated. Triggering was again achieved using the nozzle reservoir pressure transducer with a variable delay selected from the computer control system.

### PLIF Arrangement

The PLIF measurements presented here focus on detection of the OH molecule, indicating regions in the duct where ignition is occurring. Strategies for implementing such a system are discussed by Seitzman and Hanson,[12] whereas only an outline is given here. The experimental arrangement is shown in Fig. 2. The light source for the system was a Nd:YAG laser-pumped dye laser using Rhodamine 6G dye. The output was frequency doubled using a wavelength extender (WEX) system providing up to several millijoules of radiation at about 280 nm. The output is tunable allowing the selection of various rovibrational transitions in the (1,0) band of the $A^2\Sigma - X^2\Pi$ electronic transition of OH. For flow visualization, the relatively strong $R_1(10)$ line at 281.549 nm was selected. The light was formed into a 25-mm-wide sheet and passed into the test section through fused silica windows mounted in the roof of the test section and scramjet. In contrast to the other techniques presented here, PLIF provides detection of a thin slice of the flow as opposed to an integrated image across the flow. The fluorescence from this sheet was captured by the ICCD camera described in the emission section through Schott Glass UG5 and WG305 filters. These filters discriminate against flow luminosity and laser scattering, but allow passage of most of the fluorescence in the (1,1) band and the collisionally populated (0,0) band of the OH A–X transition.

Triggering of the system was carefully controlled using a computer and in-house-built electronics. The Nd:YAG laser system was required to run at 10 Hz prior to the shot to provide power stability. A signal generated by the recoil of the tunnel some 60 ms before the test time was used to disable the 10-Hz laser–trigger pulse (and after a suitable delay fire the fuel-injector). The system was then triggered from the nozzle reservoir pressure transducer, which immediately opened the CCD component of the camera, which remained sensitive for some 5 ms. Some 700 μs after the trigger, the Nd:YAG laser flashlamps were fired, and a further 280 μs later, the intensifier gate opened. After a short delay (150 ns) to allow the gate to open, the laser Q-switch was fired and the fluorescence image recorded. A gate of about 250 ns was used to discriminate as far as possible against flow emission, but to also allow for a small amount of laser jitter.

## Results

### Pressure Distributions

The existence of combustion occurring in the flow was initially investigated using the Kulite pressure transducers mounted along the floor of the duct. To distinguish between effects resulting from combustion and those caused by other flow features, experiments were performed with an air test gas and hydrogen injection, a nitrogen test gas with hydrogen injection, and lastly, an air test gas with no injection. Only minor differences were observed in the pressure traces recorded for the last two cases, and so results are only presented for the nitrogen test gas or noncombusting case and the air test gas with injection combusting case. Figure 3 shows static pressure traces in the nozzle reservoir and in the inlet of the duct for the 4-MJ/kg condition (similar traces were obtained for the higher enthalpies). The time axis in this figure is referenced from shock reflection at the entrance to the nozzle. Evident in these traces is that there is little difference between the air test gas case and the nitrogen test gas case, justifying the assumption that pressure differences in the duct can be attributed to combustion. An almost constant pressure is maintained throughout the test time, which can be considered to last in the test section from 0.7–1.5 ms after shock reflection. Prior to this time is a period where establishment of the flow occurs in the duct while the flow is terminated by driver gas contamination of the test gas. At these moderate enthalpies, the test time has been found to be longer than 1 ms from flow establishment,[13] so that contamination of the test gas by the driver gas is not thought to be a problem.

Figure 4 presents pressure variations as a function of time at various locations along the floor of the duct for the 4-MJ/kg condition. Here, pressures recorded in the air test gas case have been normalized by the corresponding values for nitrogen to provide a pressure ratio. For the nitrogen condition, a very uniform pressure was maintained throughout the test time for all transducers. In contrast, the pressure ratio seen in Fig. 4 shows sudden rises and drops on most transducers that result almost entirely from variations that occurred in the air shots. These traces appear to provide evidence of shock waves moving along the duct. These rises become more distinct as one looks further along the duct, providing evidence that combustion is occurring in the flow. The pressure levels and time behavior of these traces were very reproducible with shot-to-shot variations being at most ±10%.

The pressure distribution along the duct for the 4-MJ/kg condition is shown in Fig. 5. Each point is the average pressure over a 500-μs period beginning 1 ms after shock reflection at the entrance to the nozzle. In general, the pressures measured for the air test gas case lie above those for the nitrogen case.

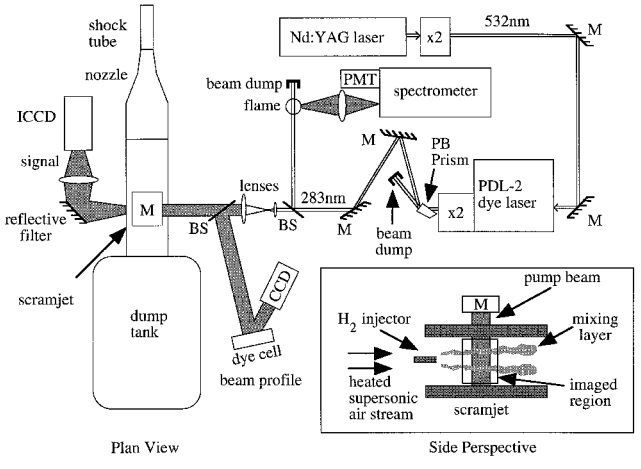


**Fig. 2 Experimental arrangement for the PLIF system. M, mirror; PB, prism–pellin–broca prism; BS, beamsplitter.**

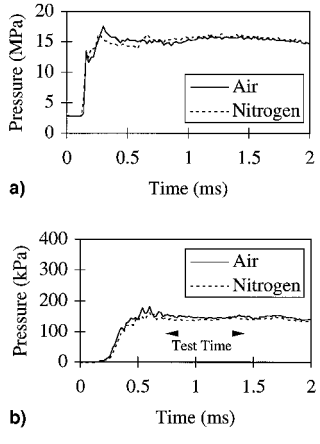


**Fig. 3 Tunnel conditions for the 4-MJ/kg condition as a function of the time from shock reflection at the entrance of the nozzle: a) nozzle reservoir pressure and b) scramjet inlet pressure.**

Particularly evident is the large pressure rise that occurs some 250-mm downstream from the injector, which will be discussed later.

To investigate combustion processes at higher enthalpies, further experiments were performed. An increase in enthalpy results in a freestream with a higher velocity but also a higher temperature (see Table 2). In addition, because of the process through which the gas is accelerated, a larger percentage of oxygen atoms are present in the freestream. Pressure traces as a function of position in the duct for the 8- and 12-MJ/kg conditions are also shown in Fig. 5. All three conditions show periodic structures with peak separations of about 70 mm. A general trend can be seen in that pressure rises are more significant toward lower enthalpies. Most significantly, the large pressure rise observed at approximately 250 mm from the injector for the 4-MJ/kg condition does not occur at the higher enthalpies. There are two effects that may explain this. An examination of the freestream conditions shows that, for the higher enthalpies, the temperature has increased above 2000 K. At these conditions, combustion becomes less efficient as a significant proportion of the products remain dissociated. Therefore, experiments that are to be conducted at higher enthalpies require a different nozzle geometry to expand the incoming gas to lower temperatures (and a similar geometric change at the inlet to a scramjet). As well, at higher enthalpies, the flow density is lower so that collisional processes leading to heat release occur less often. The relative importance of these two effects requires further investigation.

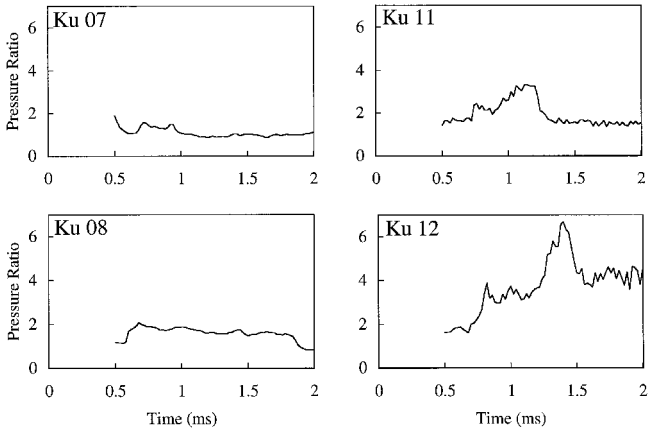


**Fig. 4 Pressure ratios (air condition divided by corresponding nitrogen condition) for selected transducers on the floor of the duct for the 4-MJ/kg condition as a function of time. Transducer positions are shown in Fig. 1.**

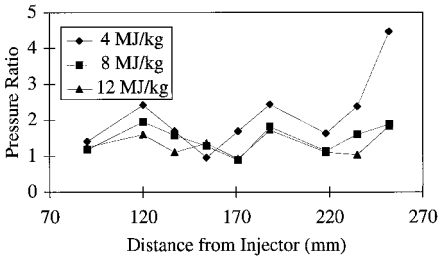


**Fig. 5 Pressure ratios (air condition divided by corresponding nitrogen condition) in the duct as a function of position for each of the conditions. Each point is an average of values over a duration of 500 μs beginning 1 ms after shock reflection.**

### Shadowgraph Imaging

Shadowgraph imaging was performed at the low-, intermediate-, and high-enthalpy conditions. However, as reflected in the pressure traces (Fig. 5), the most significant differences were observed for the low-enthalpy condition (4 MJ/kg), and only those are presented here. Images for the other conditions can be found elsewhere.[14] At this low-enthalpy condition, images were recorded at both high- and low-equivalence ratios. Shadowgraph images of the 4-MJ/kg condition given in Table 2 for air and nitrogen test gas cases are shown in Figs. 6a and 6b, respectively. In each case, flow is from left to right with injection some 30-mm upstream from the image (the height of the duct is 25 mm). The locations of the pressure measurements are also shown in the figure. The hydrogen jet as well as a series of oblique shock waves can be observed entering the left of the photograph in both cases. There are several possible sources for these waves. The shocks seen converging at the start of the image are most likely generated by a pressure mismatch that may occur when the hydrogen jet enters the flow. Other shocks may be generated by the development of boundary layers further upstream in the flow. For the nitrogen test gas case, these oblique shocks are observed to impinge on the wall just beyond pressure transducer 3 (120 mm, 38 jet diameters), and between transducers 9 (188 mm, 59 jet di-

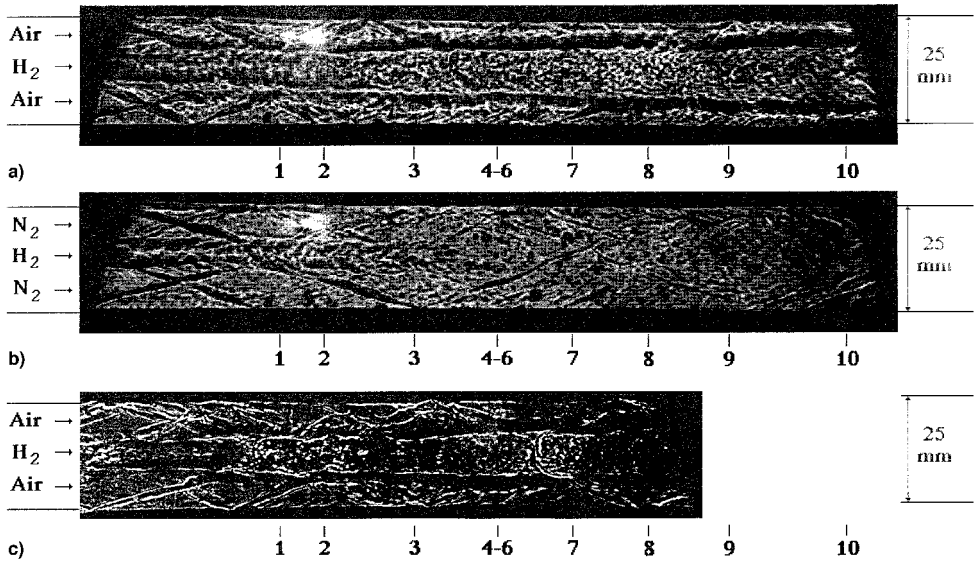


**Fig. 6 Shadowgraph images for the 4-MJ/kg condition. Flow is from left to right and the height of the duct is 25 mm. Transducer positions are shown below the images: a) air test gas, 0.92 equivalence ratio, 765-μs delay; b) nitrogen test gas, 765-μs delay; and c) air test gas, 0.5 equivalence ratio, 1022-μs delay.**

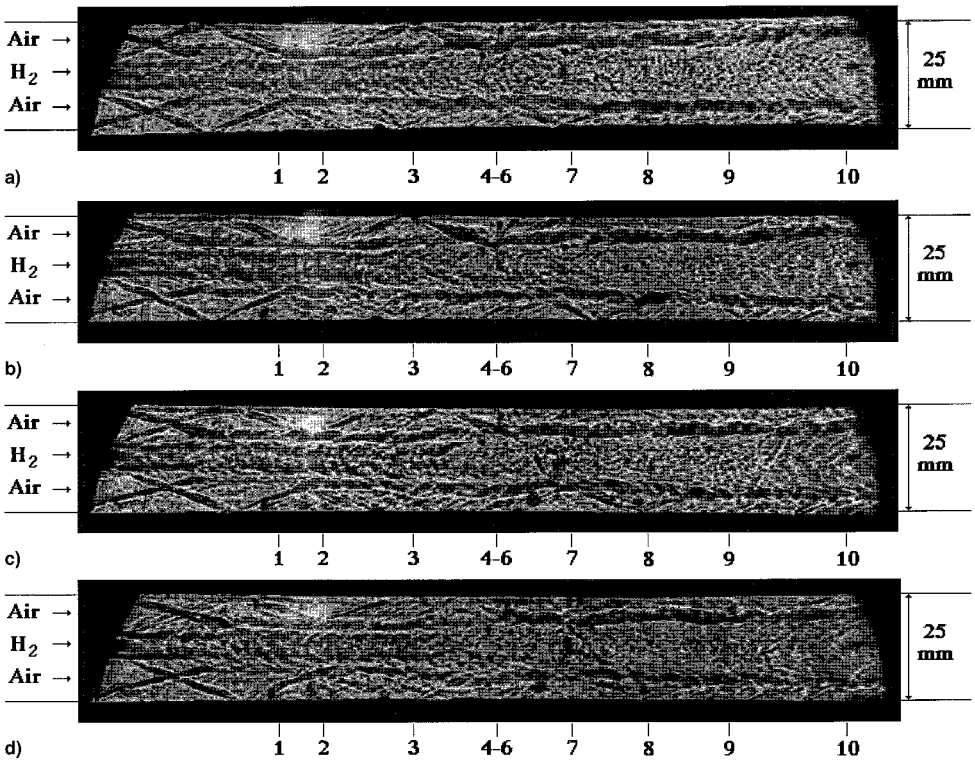


**Fig. 7 Shadowgraph images for an air test gas at the 4-MJ/kg condition with an equivalence ratio of 0.92 at various delays. Flow is from left to right and the height of the duct is 25 mm: a) 970, b) 1160, c) 1370, and d) 1590 μs.**

ameters) and 10 (218 mm, 68 jet diameters), corresponding well to the rises observed in the pressure traces for this condition (Fig. 5). The hydrogen jet is discernible for only about half the length of the duct (to about 45 jet diameters), beyond which the detection system is apparently no longer sensitive to the shear layer.

In contrast to the nitrogen case, the air test gas case shows a flow separated into three distinct regions by two layers. These layers are made visible by perturbations in the refractive index, which result from either changes in flow composition or heat release, or both. Changes in flow composition can be caused by either fuel–air mixing or chemical reactions. The chemical reactions, contributing to composition, and hence, refractive index changes, could either be induction or combustion reactions. The latter is accompanied by heat release, which perturbs the bulk flow density and, hence, refractive index. For these reasons, it is not possible to determine whether the two layers identified by the shadowgraph method are features associated with mixing, ignition, or combustion. However, the visualization of similar features close to the injector in the noncombusting case suggests that some of the perturbations must result from mixing processes. The thickness of each layer remains roughly constant along the duct, although their locations are seen to move slowly outward. Comparison of the spreading rate of the central region with the pressure distribution shown in Fig. 5 indicates that the large pressure rise observed after transducer 10 (218 mm, 68 jet diameters) corresponds well to where this layer comes close to or impacts the wall. Unfortunately, because of the geometrical restrictions, it is not possible to image this region of the flow at these conditions.

The oblique shocks present in the flow for the air test gas are observed to both reflect off the layers and also to pass through into the hydrogen, where a near normal shock is observed. This feature was observed more clearly at lower equivalence ratio conditions. Figure 6c shows one such image recorded at 4 MJ/kg with an air test gas, but with an injected equivalence ratio of 0.5. Clearly present just upstream of transducer 7 is a normal shock across the center of the duct that becomes highly oblique as it passes through the dark layer. This shock configuration is consistent with a reduction in the flow Mach number as one moves from the air to the hydrogen streams. The fact that this is not observed in the noncombusting case suggests that combustion is the cause of this effect. The locations of the oblique shocks as a function of time were traced by obtaining shadowgraph images of the flow at a number of different delay times. A series of these images for the higher equivalence ratio is shown in Fig. 7. The normal and oblique shocks were observed to move slowly backward in the duct during the test time. Good correspondence is found between the time at which the impingement point on the floor crossed the transducer locations and the pressure rises and drops were recorded. For example, Fig. 7a shows one of the generated oblique shocks impinging on transducer 7 (48 jet diameters), whereas some 200 μs later, the shock has moved downstream and the pressure on transducer 7 observed to decrease (see Fig. 4). The pressure signals observed can be explained by the shock system first moving upstream in the duct (until some 800 μs after shock reflection) and afterward moving downstream. The reason for this movement is presently unclear, although there are a number of possible sources. First, any variation in the inlet pressure may contribute to unsteadiness in the duct. Figure 3b shows this pressure measured just upstream of the injector. For both air and nitrogen conditions, the pressures are fairly constant over the test time and no correlation is seen between the time when the shock system changes from moving forward to moving back down the duct. The second possibility is that the motion is related to the combustion process. A variation in heat release could lead to a change in the pressure distribution through the duct, and hence, shifting of the position of the shocks. Since the observed reversal of motion is fairly early in the test time, it is quite possible that starting processes are influencing the conditions. Sidewall (as opposed to floor) pressure measurements were also conducted to investigate this behavior. Further details are presented in McIntyre et al.[15]

### Emission

To provide further information about the flow, emission images were recorded downstream of the injector. While the shadowgraph technique is sensitive to refractive index variations, emission measurements provide qualitative information on the temperature distribution in the flow. An emission image for the air test gas case is shown in Fig. 8. For the recording of the emission image, a Schott Glass UG5 filter was inserted in the beam path allowing transmission in the uv (200–400 nm) and near infrared (>700 nm), but blocking most of the visible radiation. Luminous-flow layers are evident in regions that coincide with the layers identified in the shadowgraph images, providing evidence that there is a temperature increase because of combustion. These layers are observed to be 20–30% larger in the emission images than those in the shadowgraph images. This probably results from a combination of focusing (the camera is focused on the center of the duct so that the edges are slightly out of focus), together with some saturation that occurred in the emission case. No such layers were observed in the nitrogen test gas case. There are a number of possible sources of this emission. Chemiluminescence because of OH has been observed in hydrogen–oxygen flames.[16] This results from the formation of OH in excited states leading to strong emission around the wavelength range of 300–320 nm. Alternatively, another possible source for this is the radiation from small traces of metallic components present in the flow that radiate more strongly at elevated temperatures. Palma et al.[17] investigated the emission from the flow in the scramjet and observed spectral lines resulting from a range of elements including iron, chromium, nickel, molybdenum, copper, tin, and aluminium. These trace elements become entrained into the flow during the period that the gas is at high temperature and pressure in the reservoir at the entrance to the nozzle. They provide concern in the application of optical techniques that measure relatively low light levels, such as laser-induced fluorescence. To investigate the relative importance of chemiluminescence and impurity emission, an image was recorded using a cutoff filter in combination with the UG5 filter to remove any contributions to the emission signal from wavelengths below about 500 nm (and, thus, OH chemiluminescence). This image also showed strong emission, lending support to the conclusion that the emission occurs primarily because of the presence of contaminant species that radiate over a wide range of wavelengths. As the intensity of radiation from such contaminants is related to temperature, this signal can thus be interpreted as a qualitative indication of temperature.

### PLIF

The location of the ignition zones was sought using PLIF. This technique detects the OH molecules that are formed through induction reactions, but may be subsequently consumed during combustion. OH is thus a suitable transient radical species that may be used for identifying where ignition is occurring. Initial PLIF measurements were unsuccessful because of the high luminosity of the flow, as evident in the emission images. To overcome these problems, further filtering in the form of a spectrally selective mirror was incorporated in the detection optics. This mirror reflects more than 80% of the incident light in the wavelength range 310–350 nm while transmitting about 90% of all other wavelengths. Results for three different 4-MJ/kg shots are presented in Fig. 9. While qualitatively similar to the emission image, it can be seen that a signal only exists over the width of the laser beam with only a low level of background emission observable outside this region. This provides clear evidence that OH is being produced in these layers (as well as for the previous conclusion that the background emission results almost solely from the presence of contaminant species). While a quantitative measurement of the OH concentration is not possible with the current arrangement, signal levels are similar in magnitude to those observed in an atmospheric pressure hydrogen–oxygen flame, indicating that the level of production in the scramjet is significant.

It should be noted that this image represents the flow only in a vertical sheet as opposed to the other techniques that measure integrated signals across the flow. This allows the detection of turbulent structures associated with significant OH densities, which can be observed in the PLIF images and are seen to vary from shot-to-shot. The outer limits of these turbulent structures align very well with the outer limits of the dark regions in the shadowgraph images. The regions of high OH density appear to coincide with both layers identified in the shadowgraph and emission images, suggesting that, since there is a change in both density and temperature in these layers, heat release occurs very soon after ignition in these regions.

The ignition time for a stoichiometric hydrogen–air flow has been estimated to be about 50 μs for a mixture at 100 kPa and 1100 K[2]. The presence of small amounts of oxygen atoms in the freestream may accelerate the process, leading to even shorter flow times. At the velocities in the duct for the 4-MJ/kg condition, this time corresponds to a distance of about 100 mm. Under the assumption that mixing occurs quickly, this would see ignition beginning near pressure transducer 2, corresponding well to the location of the beginning of the dark region in the shadowgraph images. Further PLIF imaging in this region is required to examine the onset of ignition.

The shadowgraph, emission, and PLIF images presented clearly show the development of regions within which ignition and heat release is occurring. These regions surround an inner layer, which is possibly the potential core of the flame within the scramjet. This core is observed to spread as the flow moves downstream. The core is possibly a region where very little mixing of fuel and air has occurred or where, because of the effects of the cold hydrogen, the temperature is not sufficiently high to initiate combustion. It is also interesting to note that although this core grows, the region in which combustion is occurring maintains an almost constant thickness, with changes occurring only in regions where the oblique shocks impinge on the layer. A linear fit to the outer edge of the dark region shown in Fig. 6 gives a measured shear-layer growth rate of 0.024 ± 0.008. Given that the convective Mach number in this

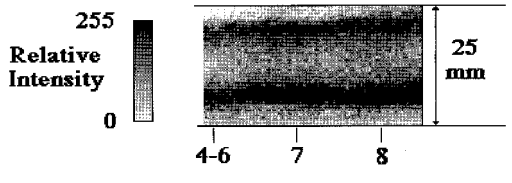


**Fig. 8 Emission image for the 4-MJ/kg air condition with an equivalence ratio of 0.92. Flow is from left to right. Transducer positions are indicated.**

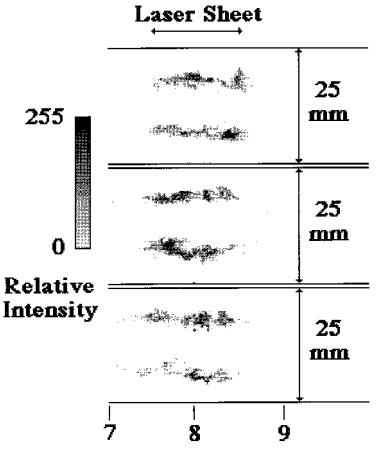


**Fig. 9 Planar laser-induced images for three 4-MJ/kg air shots with an equivalence ratio of 0.92. Flow is from left to right. Transducer positions are shown below the images.**

case is fairly low (0.2), the results in Hall et al.[1] show that one would expect the growth rates observed here to be similar to the calculated incompressible mixing-layer rates. A calculation using the parameters in Table 2 for the 4-MJ/kg condition gives this mixing rate as 0.022, in good agreement with the measured value.

While heat release is evidently occurring in these layers, the major pressure increase possibly leading to thrust was observed, by pressure measurements, to lie well downstream of the injector. This appeared to coincide with where the mixing layers impacted on the floor and roof of the duct. It is unclear from these measurements whether this corresponds to a flame front indicating major heat release, or whether it results from the generation of a strong shock because of fluid–mechanical considerations.

## Conclusions

The existence of combustion in a two-dimensional scramjet model tested in a free-piston-driven facility has been demonstrated. Pressure measurements showed significant pressure rises for the case where hydrogen was injected into an air test gas over that observed for a nitrogen test gas. This effect was most notable at low flow enthalpies where temperatures and densities were such that collisional processes were sufficient to initiate ignition leading to combustion and heat release. While the pressure measurements showed evidence that combustion was occurring, they provided little information on the extent to which the air and the hydrogen mixed. Shadowgraph images showed the existence of a narrow layer between two well-defined regions. Emission and PLIF measurements confirmed that this layer was the only region within which combustion was occurring. Comparison of the pressure measurements along the duct with the shadowgraph images leads to the conclusion that a significant pressure rise occurred where this combusting layer impacted or came close to the wall of the duct.

Further work can be divided into three sections. Of immediate interest is the visualization of the flow further downstream from the current viewing ports. The use of shadowgraph imaging and PLIF should allow a determination of the processes leading to the sudden pressure rise. A significant amount of information is also still to be obtained from the PLIF measurements. Quantitative measurements of the temperature in the mixing layer can be obtained providing a measure of the heat release in this region. Tracing of the air and hydrogen streams can also be performed by the addition of small amounts of a species detectable by PLIF such as NO or acetone.[2,18] Lastly an investigation to explore methods by which the mixing of the hydrogen into the test gas can be enhanced is planned. A number of schemes have been suggested for this purpose.

## Acknowledgments

This research has been financially supported by the Australian Research Council and NASA Grant NAGW 1467. The authors would like to thank Paul Walsh for the contribution of his technical expertise in this project. The valuable contributions from Sudhir Gai, Neil Mudford, and Sam Mallinson from the Australian Defence Force Academy and from Allan Paull, Richard Morgan, Maria Pulsonetti, and Ray Stalker from the University of Queensland are gratefully acknowledged.

## References

[1]Hall, J. L., Dimotakis, P. E., and Rosemann, H., "Experiments in Nonreacting Compressible Shear Layers," *AIAA Journal*, Vol. 31, No. 12, 1993, pp. 2247–2254.

[2]Miller, M. F., "An Experimental Investigation of the Effect of Compressibility on a Turbulent Reacting Mixing Layer," Stanford Univ., High Temperature Gas Lab., Rept. T-299, Stanford, CA, 1994.

[3]Quagliaroli, T. M., Laufer, G., Hollo, S. D., Krauss, R. H., Whitehurst, R. B., III, and McDaniel, J. C., Jr., "Planar KrF Laser-Induced OH Fluorescence Imaging in a Supersonic Combustion Tunnel," *Journal of Propulsion and Power*, Vol. 10, No. 3, 1994, pp. 377–381.

[4]Allen, M. G., Parker, T. E., Reinecke, W. G., Legner, H. H., Foutter, R. R., Rawlins, W. T., and Davis, S. J., "Fluorescence Imaging of OH and NO in a Model Supersonic Combustor," *AIAA Journal*, Vol. 31, No. 3, 1993, pp. 505–512.

[5]Casey, R. T., and Stalker, R. J., "Hydrogen Mixing and Combustion in a High-Enthalpy Hypersonic Stream," *Shock Waves @ Marseille*, Vol. 1, Springer–Verlag, 1995, pp. 321–326.

[6]Bélanger, J., and Hornung, H., "Transverse Jet Mixing and Combustion Experiments in Hypervelocity Flows," *Journal of Propulsion and Power*, Vol. 12, No. 1, 1996, pp. 186–192.

[7]Bakos, R., Tamagno, J., Trucco, R., Rizkalla, O., Chinitz, W., and Erdos, J. I., "Mixing and Combustion Studies Using Discrete Orifice Injection at Hypervelocity Flight Conditions," *Journal of Propulsion and Power*, Vol. 8, No. 6, 1992, pp. 1290–1296.

[8]Paull, A., Stalker, R. J., and Mee, D. J., "Scramjet Thrust Measurement in a Shock Tunnel," *Aeronautical Journal*, Vol. 99, No. 984, 1995, pp. 161–163.

[9]Stalker, R. J., "Development of a Hypervelocity Wind Tunnel," *Aeronautical Journal of the Royal Aeronautical Society*, Vol. 76, No. 738, 1972, pp. 374–384.

[10]McIntosh, M. K., "Computer Program for the Numerical Calculation of Frozen and Equilibrium Conditions in Shock Tunnels," Australian National Univ., Canberra, Australia, 1968.

[11]Vardavas, I., "Modelling Reactive Gas Flows Within Shock Tunnels," *Australian Journal of Physics*, Vol. 37, No. 2, 1984, pp. 157–161.

[12]Seitzman, J. M., and Hanson, R. K., "Comparison of Excitation Techniques for Quantitative Fluorescence Imaging of Reacting Flows," *AIAA Journal*, Vol. 31, No. 3, 1993, pp. 513–519.

[13]Crane, K. C. A., and Stalker, R. J., "Mass Spectrometric Analysis of Hypersonic Flows," *Journal of Physics D*, Vol. 10, No. 5, 1977, pp. 679–695.

[14]McIntyre, T. J., Rabbath, P. A. B., and Houwing, A. F. P., "Imaging of Combustion Processes in a Supersonic Combustion Ramjet," The Second Pacific International Conf. on Aerospace Science and Technology (PICAST), Melbourne, Australia, March 1995.

[15]McIntyre, T. J., Rabbath, P. A. B., and Houwing, A. F. P., "Imaging of Combustion Processes in a Supersonic Combustion Ramjet," *12th International Symposium on Air Breathing Engines*, Vol. 2, 1995, pp. 1163–1171.

[16]Davis, M. G., McGregor, W. K., and Mason, A. A., "OH Chemiluminescent Radiation from Lean Hydrogen-Oxygen Flames," *Journal of Chemical Physics*, Vol. 61, 1973, pp. 1352–1356.

[17]Palma, P. C., Houwing, A. F. P., and Sandeman, R. J., "Absolute Intensity Measurements of Impurity Emissions in a Shock Tunnel and Their Consequences for Laser-Induced Fluorescence Measurements," *Shock Waves*, Vol. 3, No. 1, 1993, pp. 49–53.

[18]Yip, B., Miller, M. F., Lozano, A., and Hanson, R. K., "A Combined OH/Acetone Planar Laser-Induced Fluorescence Technique for Visualizing Combustion Flows," *Experiments in Fluids*, Vol. 17, 1994, pp. 330–336.